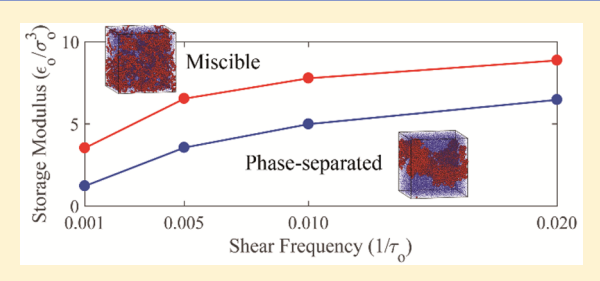
Macromolecules

Viscoelastic and Dynamic Properties of Well-Mixed and Phase-Separated Binary Polymer Blends: A Molecular Dynamics Simulation Study

Wei Peng, Raghavan Ranganathan, Pawel Keblinski, and Rahmi Ozisik*

Materials Science and Engineering, Rensselaer Polytechnic Institute, Troy, New York 12180, United States

ABSTRACT: The viscoelasticity and dynamic properties of a model dynamically asymmetric binary polymer blend are studied via molecular dynamics simulations. The model blend system is made up of two chain types having a large glass transition temperature (T_{σ}) difference and presents two blend morphologies: a well-mixed, homogeneous blend and a phase-separated blend. These two morphologies represent dynamically coupled and dynamically confined states. The well-mixed, homogeneous blend exhibited greater storage modulus and slower low-T_g matrix chain dynamics compared



to the phase-separated blend. The influence of various system parameters, such as high- T_e chain length and (volume) concentration, and shear frequency on various static, dynamic, and viscoelastic properties is investigated to identify the source of the observed stiffening in the well-mixed, homogeneous blends.

1. INTRODUCTION

Systematic research focusing on the viscoelastic properties of dynamically asymmetric polymer blends, whose two components have distinctly different dynamics, as a function of temperature and composition is an active research field. 1-7 For example, Kapnistos et al. studied rheology and phase diagram of blends consisting of polystyrene, PS, and poly(vinyl methyl ether), PVME, with a low critical solution temperature (LCST) that undergoes phase separation while the temperature is raised from 80 to 120 °C.² They found that in the homogeneous state the storage modulus decreased with increasing temperature; however, the storage modulus increased above the LCST due to phase separation.² In another study that employed a blend system with an upper critical solution temperature (UCST), a similar outcome was obtained where the phase separated state was observed to be stiffer than the miscible state.

The dynamic properties of asymmetric blend systems were also intensively studied. Entanglement-like features, such as nonexponential relaxation of Rouse normal mode autocorrelation function, were found in the unentangled polymer blends with large dynamic heterogeneity. 5,8-35 Generalized Langevin equation formalism, 9,15,16 randomized Rouse model, 13,15,18 and mode coupling theory 8,17,19,28 have been introduced to explain these abnormal dynamic properties of unentangled blends. It is commonly accepted that the increase of dynamical heterogeneity in binary blends, which could be achieved by a decrease in temperature, is responsible for the existence of entanglement-like features in unentangled blends. 8,9,15-19,28

We performed molecular dynamics simulations to study the viscoelasticity and dynamics of dynamically asymmetric polymer blends as a function of chain length, concentration, and state of miscibility (homogeneous vs. phase-separated). These simulations were inspired by the work of Senses et al.,

whose work showed thermal stiffening in poly(ethylene oxide) PEO, and poly(methyl methacrylate), PMMA, blends containing silica nanoparticles. Although the PEO/PMMA-silica nanocomposite system initially shows softening upon heating during which the storage modulus curve follows that of neat PEO, as the temperature approaches the $T_{\rm g}$ of PMMA, the system stiffens and the storage modulus first approaches and then follows that of neat PMMA. Senses et al. also showed that this thermal stiffening behavior was reversible and repeatable. This unique thermal stiffening behavior was attributed to the desorption of high- T_g PMMA chains from silica nanoparticles during the heating cycle (and adsorption during the cooling cycle).2

In the current study, a simpler system, one that is made up of a dynamically asymmetric polymer blend, was chosen to explore the hypothesis provided by Senses et al. During molecular dynamics simulations, the blend system was designed to exhibit heterogeneous dynamics by manipulating the stiffness of the two chains such that the matrix chains have a low $T_{\rm g}$ and the minority chains have a high $T_{\rm g}$.

2. THEORETICAL BACKGROUND

In this section, theories such as randomized Rouse model and generalized Langevin formalism are briefly introduced to provide the necessary background on heterogeneous polymer blends.

2.1. Rouse Model. In the Rouse model, a linear polymer chain is represented by N beads, which interact with neighboring beads through an entropic spring with a spring

Received: March 29, 2017 Revised: June 7, 2017 Published: August 1, 2017

constant of $\sim 3k_{\rm B}T/b^2$ ($k_{\rm B}$ is the Boltzmann constant, T is temperature, and b is the bond length) and experience stochastic forces, $f_n(t)$, from the surrounding environment. The stochastic forces have a Gaussian distribution and satisfy the following conditions:

$$\langle f_n(t) \rangle = 0 \tag{1}$$

$$\langle f_{n\alpha}(t) \cdot f_{m\beta}(t') \rangle = 2k_{\rm B}T\zeta_0 \delta_{nm} \delta_{\alpha\beta} \delta(t - t')$$
(2)

where ζ_0 is the friction constant, δ is the Kronecker delta function, indices n and m represent chains, and α and β represent Cartesian axes. Equations 1 and 2 show that friction forces imposed by environment onto chains are spatially and temporally uncorrelated. The Langevin equation becomes a linear equation of the coordinates of chain beads, $\mathbf{R}(t)$.

$$\zeta_0 \frac{dR_n(t)}{dt} = -\frac{3k_B T}{b^2} [2\mathbf{R}_n(t) - \mathbf{R}_{n-1}(t) - \mathbf{R}_{n+1}(t)] + f_n(t)$$
(3)

The solution of eq 3 yields the following:

$$X_{p\alpha}(t) = \frac{1}{N} \sum_{i=1}^{N} \left\{ R_{i\alpha}(t) \cos\left[\left(i - \frac{1}{2}\right) \frac{p\pi}{N}\right] \right\}$$
(4)

where Rouse mode index, p, ranges between 0 and N-1. The time autocorrelation function of normal modes can be used to characterize the relaxation of Rouse chains. For example, when p=0, the following equation is obtained:

$$\langle [X_{0\alpha}(t) - X_{0\alpha}(0)] \cdot [X_{0\beta}(t) - X_{0\beta}(0)] \rangle = \delta_{\alpha\beta} \frac{2k_{\rm B}T}{N\zeta_0} t$$

This autocorrelation function corresponds to diffusion of the center of mass (COM) of Rouse chains, and the diffusion coefficient becomes $k_{\rm B}T/N\zeta_0$.

For p > 0

$$\langle X_{p\alpha}(t) \cdot X_{q\beta}(0) \rangle = \delta_{pq} \delta_{\alpha\beta} \frac{k_{\rm B}T}{k_p} \exp\left(-\frac{t}{\tau_p}\right)$$
 (6)

where

$$k_p = \frac{6\pi^2 k_{\rm B}T}{Nb^2} p^2$$
 and $\tau_p = \frac{\zeta_0 N^2 b^2}{3\pi^2 k_{\rm B} T p^2}$ (7)

These autocorrelation functions correspond to different relaxation modes with wavelengths of N/p. It can be seen that the relaxation time, τ_p , is proportional to p^{-2} . The power-law relation $\tau_p \sim p^{-x}$ holds in neat melts and dynamically asymmetric blends, but the exponent increases with increasing heterogeneity in dynamically asymmetric blends.

2.2. Randomized Rouse Model. In the randomized Rouse model, the friction coefficient follows a log-normal distribution centered around the average mobility obtained from experimental 15,18

$$f(\zeta, \zeta_0, \sigma) = \frac{1}{\zeta \sigma \sqrt{2\pi}} \exp \left[-\frac{(\ln \zeta - \ln \zeta_0)^2}{2\sigma^2} \right]$$
(8)

where σ is the distribution width and is the only fitting variable, and ζ_0 is the average friction coefficient obtained from experiments, such as neutron backscattering. ^{15,18} In this

model, the space and time correlation functions of friction forces are still neglected. Then the Langevin equation becomes

$$\frac{\mathrm{d}R_n(t)}{\mathrm{d}t} = \sum_{m=0}^{N-1} L_{nm} \left\{ \frac{3k_{\rm B}T}{b^2} [R_{n+1}(t) - 2R_n(t) + R_{n-1}] + f(m, t) \right\} \tag{9}$$

where $L_{mn}=1/\zeta_n\delta_{mn}$ is the diagonal mobility matrix. This Langevin equation can be solved semi-analytically by varying distribution width, $\sigma^{.15,18}$ When the friction coefficient distribution is wider, which means higher dynamical heterogeneity, the relaxation time of normal mode correlation function shows greater power-law exponent x ($\tau_p \sim p^{-x}$). A very similar feature is observed in entangled polymer melts and blends. 27,31,32

2.3. Generalized Langevin Equation. In the generalized Langevin equation formalism, the memory kernel represents the spatial and temporal correlation of friction forces imposed against the tagged chains from surrounding environment. Following the formalism proposed by Schweizer²⁸ and Colmenero,⁹ the integro-differential equation of normal mode of the faster moving (softer) component in the polymer blend can be written as follows:

$$\zeta_0 \frac{dX_p(t)}{dt} + \int_0^t dt' \, \Gamma_p(t-t') \frac{dX_p(t')}{dt'} = -\frac{\zeta_0}{\tau_p^0} X_p(t) + F_p(t)$$
(10)

where $\Gamma_p(t)$ is the memory function. Considering that $\langle X_p(0) \cdot F_p(t) \rangle = 0$, a similar integro-differential equation can be deduced from eq 10:

$$\begin{split} \frac{\mathrm{d}\langle X_p(0)X_p(t)\rangle}{\mathrm{d}t} &+ \frac{1}{\zeta_0} \int_0^t \mathrm{d}t' \, \Gamma_p(t-t') \frac{\mathrm{d}\langle X_p(t')X_p(0)\rangle}{\mathrm{d}t'} \\ &= -\frac{\langle X_p(0)X_p(t)\rangle}{\tau_p^0} \end{split} \tag{11}$$

If only long wavelength relaxation of softer component is taken into account, it can be assumed that the memory kernel decays much faster than the time correlation functions of normal modes of softer chains. Then, the integral in eq 11 can be approximated by the following product:

$$\int_{0}^{t} dt' \, \Gamma_{p}(t-t') \frac{d\langle X_{p}(t')X_{p}(0)\rangle}{dt'}$$

$$= \frac{d\langle X_{p}(t')X_{p}(0)\rangle}{dt'} \int_{0}^{t} dt' \, \Gamma_{p}(t-t')$$
(12)

And eq 11 can be solved as follows:

$$\frac{\langle X_p(t)X_p(0)\rangle}{\langle X_p(0)X_p(0)\rangle} = \exp\left[-\frac{\zeta_0}{\tau_p^0} \int_0^t \frac{\mathrm{d}t'}{\zeta_0 + \zeta(t')}\right] \tag{13}$$

where $\zeta(t)$ is the extra friction force caused by the memory kernel and is defined by the following equation:

$$\zeta(t) = \int_0^t \Gamma(t') dt'$$
(14)

For classical Rouse mode, $\zeta(t)$ vanishes, and therefore eq 13 is reduced to the well-known exponential decay function. As long as the heterogeneity in the dynamics of the system is large enough, $\zeta(t)$ could significantly influence the denominator of the integral in eq 13, resulting in a nonexponential decay of

normal mode correlation functions. A stretched exponential decay can be a good approximation for the numerator term in

$$\langle X_p(t)X_p(0)\rangle \approx \exp\left[-\frac{t}{\tau_p'}\right]^{\beta}$$
 (15)

In eq 15, the stretch exponent, β , should be less than unity, and the relaxation time τ_p' should follow the power-law relation (τ_p $\sim p^{-x}$) of a new exponent x, which could be used to characterize the dynamics heterogeneity of the system-a greater exponent corresponds to a greater degree of system heterogeneity.

3. SIMULATION METHODOLOGY

3.1. Polymer Chain Structure and Force Field. In the current study, polymer chains are described by a united atom model, where adjacent "beads" representing units of polymer chains are connected by finitely extensible nonlinear elastic (FENE) bonds.²⁷ Nonbonded pairwise interactions between beads are described by a shifted Lennard-Jones (LJ) potential:

$$U_{\text{shifted LJ}} = \begin{cases} 4\varepsilon_0 \left[\left(\frac{\sigma_0}{r} \right)^{12} - \left(\frac{\sigma_0}{r} \right)^6 - \left(\frac{\sigma_0}{r_c} \right)^{12} + \left(\frac{\sigma_0}{r_c} \right)^6 \right] & r < r_c \\ 0 & r \ge r_c \end{cases}$$

$$(16)$$

where r is the distance between nonbonded beads, σ_0 is the distance between two beads where the potential energy is equal to zero, r_c (= 2.5 σ_0) is the cutoff, and ε_0 is the energy well depth. The average FENE bond length b is $0.97\sigma_0$. In order to create two different polymer chains exhibiting different dynamics, the bonded interactions between adjacent beads in one type of chain was described by FENE and LI potentials, whereas the second type of chain included many-body bending and torsional terms in addition to FENE and LI interactions. For both types of chains, all nonbonded interactions were described by LJ interactions. These two different chains were referred to as A (stiffer chains using FENE, LJ, and many-body interactions) and B (softer chains using only FENE and LJ). Throughout the current study, softer B chains form the matrix into which stiffer A chains are added at varying concentrations. The glass transition temperatures of neat A $(N_A = 50)$ and neat **B** $(N_{\rm B}=50)$ are $1.2-1.5\varepsilon_{\rm 0}/k_{\rm B}$ and $\sim 0.45\varepsilon_{\rm 0}/k_{\rm B}$ $(\varepsilon_{\rm 0}/k_{\rm B}$ is the reduced unit for temperature), respectively.

For the stiffer A chains, the angle potential between three adjacent A beads within the same chain is defined as follows:

$$U_{\theta} = K_{\theta}(\theta - \theta_0)^2 \tag{17}$$

where θ is the bond angle, θ_0 (=120°) is the equilibrium bond angle, and $K_{\theta} = 60\varepsilon_0/\sigma_0^2$. In addition, a torsional potential was used to make A chains even stiffer compared to B chains.

$$U_{\phi} = K_{\phi}(1 + \cos 2\phi) \tag{18}$$

where ϕ is the torsion angle and $K_{\phi} = 40\varepsilon_0/\sigma_0^2$. The entanglement length, $N_{\rm e}$, for softer **B** chains was reported to be 85,³³ while for **A** chains with many-body interactions, the entanglement length was reported to be between 28 and 45.34,35 In the current study, the length of B chains (N_B) was kept constant at 50 and the length of A chains (N_A) was varied from 3 to 100. All simulations were performed with the Large-scale Atomic/Molecular Massively Parallel Simulator (LAMMPS), ³⁶ and the visualization of the simulation box is performed via OVITO.37

3.2. Model Structures. In all simulations, the total number of beads was kept as close to 40 000 as possible, and the masses of A and B beads are the same. Two distinct structures corresponding to a well-dispersed blend and a phase-separated blend were prepared. These two distinct structures are referred to as "mixed" and "unmixed", respectively, throughout the article. Mixed blend structures were prepared by the following procedure. Chains were randomly placed into the simulation box with periodic boundary conditions turned on. Since it is possible for beads to overlap with each other initially, a special pairwise interaction (a "soft potential") was temporarily applied to remove overlaps (see "unoverlap" procedure in the LAMMPS documentation). These initial systems were run at constant volume for 1 million time steps with a time step (Δt) of $0.005\tau'$ (where τ' is the reduced time unit, $\tau' = \sigma_0 \sqrt{m_0/\varepsilon_0}$), with a Langevin thermostat during which the magnitude of the soft potential was gradually ramped up. After all overlaps were eliminated, nonbonded pairwise potential was switched to the shifted LJ potential (with $\varepsilon_{AA} = \varepsilon_{AB} = \varepsilon_{BB} = \varepsilon_0$ and $\sigma_{AA} = \sigma_{AB} = \varepsilon_0$ $\sigma_{\rm BB} = \sigma_0$), and the systems were run at constant pressure (P = 0) and temperature $(T = 0.5\varepsilon_0/k_B)$ for 5 million steps with a time step of $0.005\tau'$. Then many-body interactions for all A chains were turned on and the simulations were performed with an NPT ensemble for 40–100 million steps using a time step of $0.005\tau'$. Production runs were performed until chains move, on average, a distance that is equal to their average radius of gyration (R_{α}) .

To prepare unmixed blends, after the overlaps were removed, a shifted LJ potential with ε_{AA} = $10\varepsilon_0$ was applied to all A-A bead interactions, while keeping $\varepsilon_{AB} = \varepsilon_{BB} = \varepsilon_0$. Under this setting, the phase separation is induced enthalpically. These systems were simulated with an NPT ensemble at a higher temperature of $2.0\varepsilon_0/k_{\rm B}$ for 2 million steps. At this temperature, beads have enough mobility to drive the system to phase separation. Then the LJ potential was shifted back to $\varepsilon_{\rm AA}$ = $\varepsilon_{\rm AB}$ = $\varepsilon_{\rm BB}$ = $\varepsilon_{\rm 0}$, and the temperature of the system was reduced to $0.5\varepsilon_0/k_{\rm B}$. Once the temperature is lowered and the LJ potential is switched back, the phase-separated morphology persists because of the slow kinetics at the lower temperature. Finally, many-body interactions for A chains were turned on, and all systems were equilibrated with an NPT ensemble for 40-100 million steps. Unmixed system production runs were performed in the same way as was done for the mixed blend systems. In the current work, the production runs were always performed at a constant temperature of $0.5\varepsilon_0/k_{\rm B}$ in order to kinetically arrest both mixed and unmixed morphologies. The snapshots of the mixed and unmixed blends are shown in Figure 1.

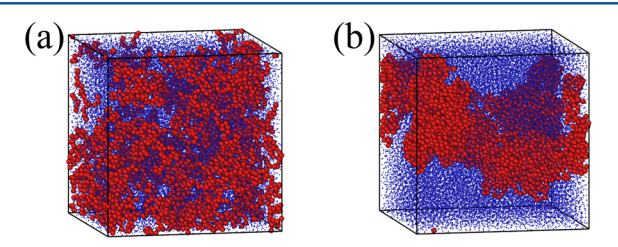


Figure 1. Snapshots of (a) mixed and (b) unmixed blend configurations. Red spheres represent A chain beads, and blue spheres represent B chain beads.

3.3. Analysis of Dynamics and Viscoelasticity. 3.3.1. Analysis of Dynamics. Mean-squared displacement (MSD) and Rouse mode analysis were used to characterize the dynamics of polymer chains and beads. For all blend systems, five independent samples were simulated using an NVE ensemble with a time step of $0.001\tau'$ after equilibrating each system using an NPT ensemble. The coordinates of beads and chain center of masses were recorded to calculate bead and COM MSDs and autocorrelation function of Rouse modes. MSDs and Rouse mode autocorrelation functions within each time interval were averaged over multiple time windows of different time origins. MSDs and Rouse autocorrelation functions were calculated from successive NVE simulations, and the kinetically arrested structures did not show any aging

(changes in morphology) on the time scale of our simulations. 3.3.2. Oscillatory Shear Deformation. It is well-known that study of viscoelasticity of polymers by equilibrium molecular dynamics (EMD) simulations often suffers from the problem of convergence of stress autocorrelation.³⁸ In the current work, the viscoelasticity of polymer blend systems was studied via oscillatory shear flow implemented by SLLOD equations of motion,³⁹ equivalent to Lees—Edwards "sliding brick" boundary conditions.⁴⁰ Operationally, the upper plane (z-axis plane) of the simulation box was shifted parallel to the lower plane along the x-axis, such that each point in the box has a "streaming velocity" along the x-axis direction with a linear gradient along the y-axis direction. These streaming velocities were subtracted when the temperature of the system was calculated. This way an oscillatory shear was imposed on the system as follows:

$$\gamma_{xy} = \gamma_0 \sin(2\pi f t) \tag{19}$$

where γ_0 (= 0.02) is the oscillatory shear amplitude and f is shear frequency ranging from $0.001\tau'$ to $0.02/\tau'$. Each nonequilibrium molecular dynamics (NEMD) simulation contained at least 20 oscillatory shear cycles, and the virial shear stresses, τ_{xy} , of the whole system were recorded every five time steps. The shear stress was fitted by the linear viscoelasticity equation:

$$\tau_{xy} = \tau_0 \sin(2\pi f t + \delta)$$

$$= \tau_0 \cos(\delta) \sin(2\pi f t) + \tau_0 \sin(\delta) \cos(2\pi f t)$$
(20)

where τ_0 is the shear stress amplitude and δ is the phase shift. Storage (G') and loss (G'') moduli are defined as follows:

$$G' = \frac{\tau_0 \cos(\delta)}{\gamma_0} \tag{21a}$$

$$G'' = \frac{\tau_0 \sin(\delta)}{\gamma_0} \tag{21b}$$

In addition, by calculating the virial shear stress associated with every bead, it is possible to monitor stress for each blend component (τ_A or τ_B), and the corresponding storage and loss moduli. Of course, it is assumed that each blend component experiences the same shear strain as the whole system. Note that during the oscillatory shear deformation, we found that the number of contacts between A and B beads in unmixed blends did not change significantly, so the conformation of unmixed blends could persist during the oscillatory shear.

4. RESULTS AND DISCUSSION

4.1. Static Properties. Static properties of the polymer chains are important to have a better understanding of the viscoelastic and dynamic properties. The radial distribution function of A–B bead contacts, $\rho_{AB}(r)$, were calculated for mixed and unmixed blend configurations (not shown). The integral under the first peak in $\rho_{AB}(r)$ gives the number of A–B contacts. For blends with $N_A = N_B = 50$ and $X_A = 0.1$, the average number of A–B contacts in the unmixed and mixed blends was 5.44 and 9.22, respectively, and therefore there are significantly more interactions between the high- and low- T_g chains in the mixed blends. This observation is key to understanding the stiffening behavior observed in the mixed blend, which will be discussed in section 4.2.

The dependence of the normalized radius of gyration of high- $T_{\rm g}$ A chains, $\langle R_{\rm g}^2 \rangle/(N_{\rm A}b^2)$, on $N_{\rm A}$ at various blend concentrations is presented in Figure 2. When $N_{\rm A}$ is less than

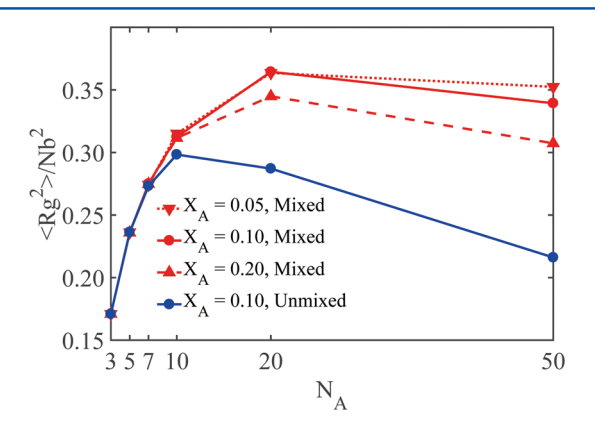


Figure 2. Normalized radius of gyration $(\langle R_g^2 \rangle / (N_A b^2))$ of **A** chains in mixed and unmixed blends as a function of **A** chain length (N_A) at various concentrations.

10, $\langle R_{\rm g}^2 \rangle / (N_{\rm A} b^2)$ increases almost linearly with $N_{\rm A}$, and no effect of morphology (mixed vs unmixed) or concentration is observed, suggesting that short chains are rigid regardless of concentration or morphology. For $N_{\rm A} > 20$, the high- $T_{\rm g}$ A chains seem to become more flexible, and a strong dependence on concentration and blend morphology is observed. Interestingly, high- $T_{\rm g}$ A chains become more flexible (or approach that of ideal chain behavior faster) with increasing A chain concentration $(X_{\rm A})$. At the same A chain concentration $(X_{\rm A} = 0.1)$, high- $T_{\rm g}$ A chains approach ideal behavior faster in the unmixed blend compared to mixed blend. These two observations suggest that high- $T_{\rm g}$ A chains behave like ideal chains or become more flexible when there are more high- $T_{\rm g}$ A chains in their local environment.

4.2. Viscoelasticity Analysis. The phase shifts and storage moduli of A–B blends and neat melts of A and B chains as a function of shear frequency are presented in Figure 3. The viscoelastic properties of neat high- $T_{\rm g}$ polymer A are almost frequency-independent (within the frequency range studied) with a phase shift of \sim 5°, which indicates that neat polymer A is rather elastic, which is not surprising considering that this polymer is well below its glass transition temperature. By contrast, the moduli and phase shift of low- $T_{\rm g}$ neat polymer B exhibits strong frequency dependence and a highly viscous behavior, particularly at low frequencies. Interestingly, the storage moduli of neat polymer B approaches to that of polymer A at high frequencies. We attribute this to the fact that

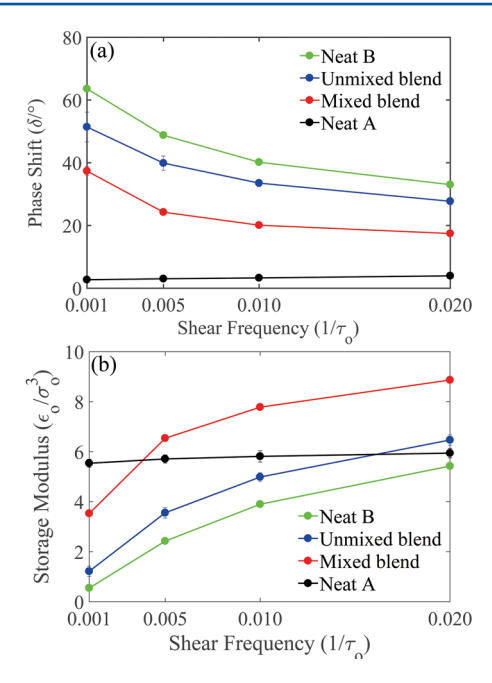


Figure 3. (a) Phase shifts and (b) storage modulus of neat polymer **A** and **B** and blends (mixed and unmixed) of **A** and **B** chains as a function of shear frequency. $N_A = N_B = 50$ and $X_A = 0.1$ for all blends.

while the A chains are more rigid, the B chains have higher density, leading to similar modulus at high frequencies.

As expected, the phase shifts of both mixed and unmixed blends are within the range delineated by phase shifts of the low- and high- $T_{\rm g}$ neat polymers. The same is true for storage moduli but only at the low frequency range. Also, the phase shifts and storage moduli of both the mixed and unmixed blends show a strong frequency dependence similar to that exhibited by neat low- $T_{\rm g}$ B polymer.

The most striking observation is that across the whole frequency range the storage modulus of the mixed blend is greater than that of the unmixed blend. Conformation related stiffening was observed in similar systems experimentally. For example, in a study performed on polystyrene (PS) and PVME blends, Kapnistos et al.² observed that phase separation led to stiffening, which was attributed to the formation of interfaces between stiff PS and soft PVME domains. In the current study, the comparison is performed at the same temperature (below the T_g of the high- T_g component but above the T_g of the low- T_{g} component) for both mixed and unmixed systems; however, the mixed system presents a greater modulus than the unmixed system, which is the opposite of what Kapnistos et al. presented. In the subsequent sections, we will provide a number of observations aimed at elucidating the underlying physics leading to the greater stiffening observed in the mixed blend compared to the unmixed blend.

4.3. Chain Diffusion and Non-Gaussianity Parameter. The center of mass (COM) and monomer (bead) mean-square displacements (MSDs) of low- $T_{\rm g}$ B chains as a function of time are shown in Figure 4. At short time scales ($t < 0.1\tau'$), bead MSDs show ballistic dynamics both in the neat B melt and in the mixed and unmixed blends. The mixed and unmixed blends' MSDs start deviating from that of the neat B melt around $t \sim 1-10\tau'$, which can be attributed to the presence of A chains and their effect on the dynamics of B chains in the blends. However, it is clear that blend morphology has an

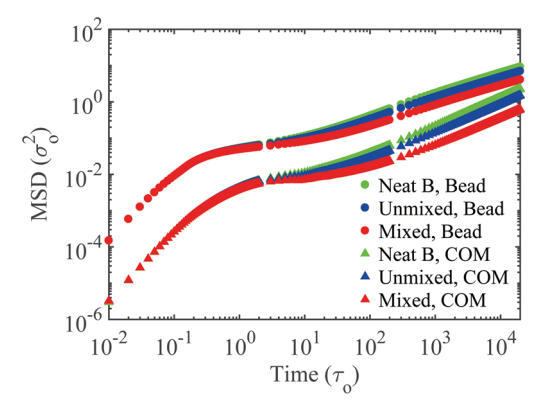


Figure 4. Comparison of the center of mass (COM) and monomer (bead) mean-square displacements (MSDs) of **B** chains in neat **B** melt and A/B blends. $N_A = N_B = 50$ and $X_A = 0.1$ for blends.

important role on the MSDs of B chains, since B chain MSDs in mixed and unmixed blends exhibit significant differences.

At long time scales $(t/\tau' > 1000)$, the MSDs of B beads in both neat B melt and blends show a clear power-law $\sim t^x$ dependence on time, where x=0.56-0.58, which is consistent with the Rouse behavior (for which x=0.5). The power-law exponent for the COM MSD ranges between 0.6 and 0.8, which is in agreement with the literature. Most interestingly, we observe that diffusion of B chains is slowed down by A chains in the mixed blend more significantly than in the unmixed blend. This and previous observations suggest that the high- $T_{\rm g}$ A chains act as obstacles to the movement of low- $T_{\rm g}$ B chains, and the A chains are more effective obstacles in the mixed blends than they are in the unmixed blend.

The non-Gaussianity parameters (α_2) of B beads in the pure B melt and in mixed and unmixed blends as a function of

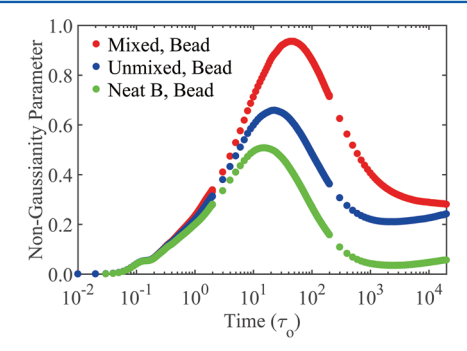


Figure 5. Non-Gaussianity parameters of **B** beads in neat **B** melt and in mixed and unmixed blends. $N_{\rm A}=N_{\rm B}=50$ and $X_{\rm A}=0.1$ for blends.

simulation time are shown in Figure 5. The non-Gaussianity parameter is defined as follows:²⁶

$$\alpha_2(t) = \frac{3\langle r^4(t)\rangle}{5\langle r^2(t)\rangle^2} - 1 \tag{22}$$

and is a measure of heterogeneity in dynamics. In both the neat B melt and blend systems, the non-Gaussianity parameters display two peaks: a small peak at $t/\tau' \sim 0.1$ and a strong peak within $t/\tau' \sim 10-100$. The position and intensity of the first peak are the same for all systems, whereas the second peak position and intensity depend on the system configuration as follows:

$$\alpha_2 = \begin{cases} \sim 0.50 & t/\tau_0 \sim 10{-}20 & \text{neat } \mathbf{B} \text{ melt} \\ \sim 0.65 & t/\tau_0 \sim 30{-}40 & \text{unmixed blend} \\ \sim 0.95 & t/\tau_0 \sim 40{-}50 & \text{mixed blend} \end{cases} \tag{23}$$

The first peak position is related to the displacements of B beads at small time scales $(t/\tau' < 0.1)$ and is associated with the influence of local environment on the short wavelength relaxation of B beads. All three systems show the same intensity and peak distribution, which indicates that the dynamics of the B beads are not influenced by the presence of A chains in these short time scales. In addition, the displacements of B beads follow a Gaussian distribution because α_2 is almost zero.

The dependence of the second peak position and intensity on system configuration is clearly influenced by the presence and dispersion state of A chains within the B matrix. The non-Gaussianity parameter of B beads is greatest in the mixed blend system, suggesting that B beads in this system experience the greatest dynamic heterogeneity (Figure 5). At long time scales $(t/\tau' > 1000)$, non-Gaussianity parameter of B beads in the neat B melt vanishes; however, for the two blend systems, dynamic heterogeneity persists, and the non-Gaussianity of B beads in the unmixed blend approaches to that in the mixed blend. This is an interesting observation because it suggests that although the unmixed blend remains unmixed, the nature of the interactions of A and B beads at the A/B interfaces is similar in both mixed and unmixed blends.

4.4. Rouse Mode Analysis. Rouse mode analysis was performed to get further insight into the influence of high- $T_{\rm g}$ A chains on the dynamics of low- $T_{\rm g}$ B chains. Figure 6 shows the

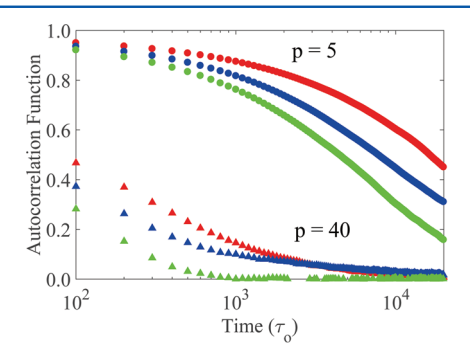


Figure 6. Rouse normal mode autocorrelation functions of **B** beads in neat **B** melt and in A/B blends. Red, blue, and green filled symbols correspond to mixed blend, unmixed blend, and neat **B** melt, respectively. Circles represent p = 5 and triangles represent p = 40. $N_A = N_B = 50$ and $X_A = 0.1$ for blends.

Rouse normal mode autocorrelation functions of B chains in neat B melt and blend systems as a function of time. These functions were fitted by eq 15 to obtain stretch exponents (β) and relaxation times (τ_p) . Only the data from long time scales $(t/\tau'>100)$ were used during fitting. All three systems show nonexponential decay and have different stretch exponents. Nonexponential decay for pure melts and blends was also observed in the literature. Some modes autocorrelation functions of B chains decay slower in the blends than in the neat B melt for various modes (p=5 and 40). In addition, B chains relax slower in the mixed blend compared to those in the unmixed blend.

Figure 7 shows the relaxation time as a function of relaxation wavelength (N_B/p) . For the neat B melt chains, the power-law

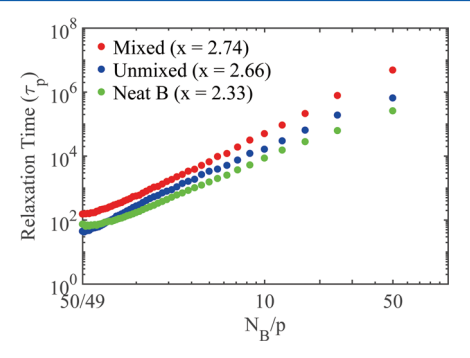


Figure 7. Rouse relaxation times of **B** beads in neat **B** melt and in **A/B** blends with corresponding power-law exponents $(\tau_p \sim p^{-x})$ as a function of N_B/p . $N_A = N_B = 50$ and $X_A = 0.1$ for blends.

exponent x ($\tau_p \sim p^{-x}$) was found to be equal to ~2.33, which is consistent with that obtained by Brodeck. In the mixed blend system, the power-law exponent x equals ~2.74, which is greater than that of the unmixed blend (~2.66). Brodeck et al. found that the power-law exponent increases from 2.2 to 3.5 when temperature was lowered from 1.5 to 0.33 as a result of increasing heterogeneity in dynamics.

4.5. Mechanism of Stiffening. *4.5.1. Effect of High-T_g Chain Length.* As discussed in section 3.3.2, the viscoelasticity of polymer blends can be decomposed into contributions from each blend component. Results presented so far clearly showed that mixed blends were stiffer than unmixed blends. In view of these two observations, it is possible to ask which of the two components (A or B) in the mixed blends is responsible for the observed stiffening behavior. To answer this question, storage moduli of blends was decomposed into A (G'_A) and B (G'_B) contributions as shown in Figure 8, from which the following

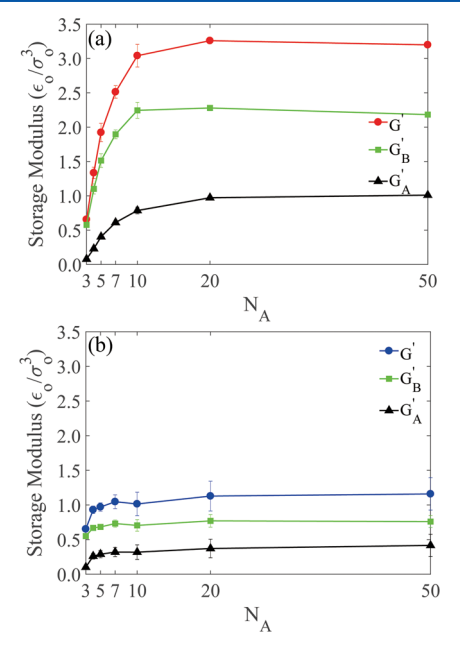


Figure 8. Storage moduli as a function of **A** chain length in (a) mixed and (b) unmixed blends. Circles, squares, and triangles represent total, **B**, and **A** portion of storage modulus, respectively. $X_{\rm A}=0.1$ and $f=0.001/\tau_0$.

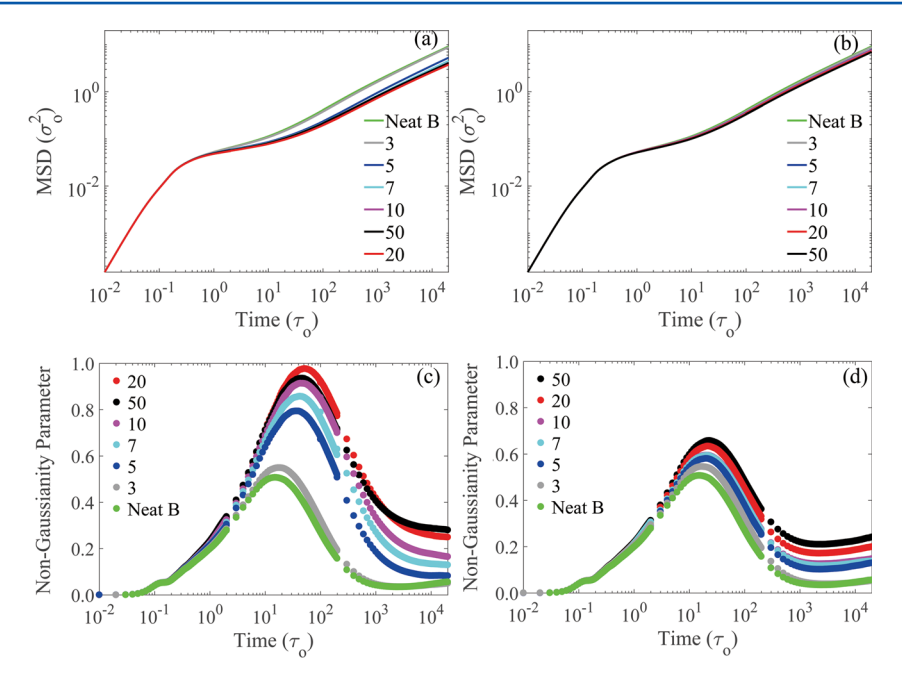


Figure 9. (a, b) MSDs of low- T_g B beads in (a) mixed and (b) unmixed blends. (c, d) Non-Gaussianity parameters of low- T_g B beads in (c) mixed and (d) unmixed blends. Neat $\ddot{\mathbf{B}}$ melt result is also presented. Variation of N_A is indicated in each figure. $X_A = 0.1$ for blends.

observations can be made: (i) The overall shear stress is dominated by the flexible, low- $T_{\rm g}$ B chains rather than the stiffer, high- $T_{\rm g}$ A chains—this is expected since A chains constitute a small fraction of the system. (ii) Both $G_{\rm A}'$ and $G_{\rm B}'$ of the mixed blend are greater than those of the unmixed blend. (iii) $G_{\rm A}'$ and $G_{\rm B}'$ of unmixed blends are almost independent of A chain length $(N_{\rm A})$; however, $G_{\rm A}'$ and $G_{\rm B}'$ of the mixed blends strongly depend on $N_{\rm A}$ particularly for $N_{\rm A} < 20$.

MSD and non-Gaussianity parameters of B beads in mixed and unmixed blend systems as a function of $N_{\rm A}$ are presented in Figure 9. It is clear that MSD and non-Gaussianity parameter of B beads in the mixed blends depend more strongly on $N_{\rm A}$ compared to those in the unmixed blends. When $N_{\rm A}$ increases from 3 to 20, motion of B beads becomes slower in the mixed blends. However, B beads diffuse faster when $N_{\rm A}$ increases from 20 to 50.

We speculate that the origin of these observations is the following: As $N_{\rm A}$ increases, the mobility of A chains decreases dramatically, which makes A chains act as immobile obstacles to B chains. However, further increase in $N_{\rm A}$ results in more interactions of A beads among themselves, resulting in fewer interactions between A and B beads. That is probably why we can see that with increasing $N_{\rm A}$, the mobility of B chains first decreases and then increases.

Figure 10a shows the center of mass (COM) MSDs of A and B chains in the mixed blends as a function of time for various $N_{\rm A}$. Interestingly, it can be seen that when A chains are shorter than 20, the COM of A chains diffuse faster than B chains. However, comparison of COM MSDs of chains having different chain lengths can be a bit misleading. Therefore, in Figure 10b we present the MSDs of A and B beads in the mixed blends. First, we note that when A chain length is 3, A beads move slower than B beads at short time scales ($t < \sim 1000\tau'$) and faster at long time scales ($t > \sim 1000\tau'$). Therefore, when $N_{\rm A} = 3$, A chains are not very effective obstacles for B chain motion. When A chain length ranges from 5 to 10, A beads move slower than B beads at all times accessible in simulations. However, at long time scales ($t > \sim 1000\tau'$), the slope of MSD

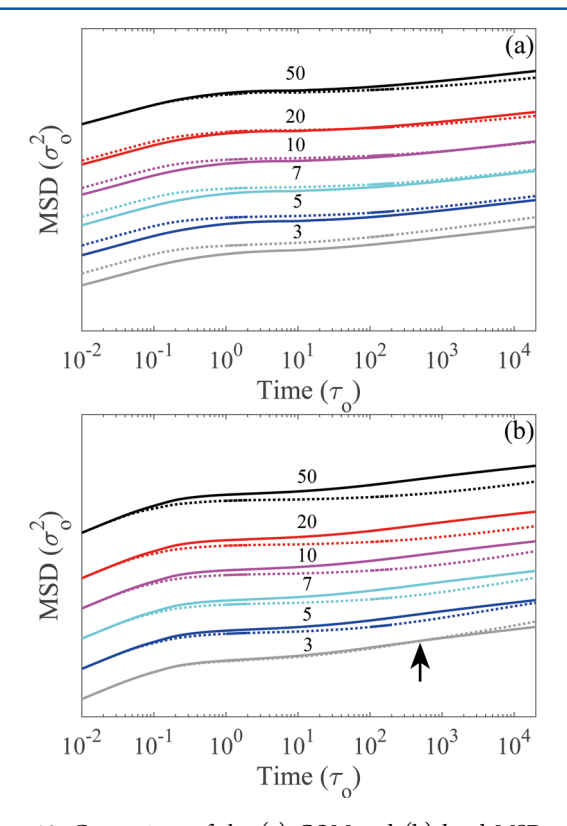


Figure 10. Comparison of the (a) COM and (b) bead MSDs of A (dashed lines) and B (solid lines) chains in mixed blends as a function of N_A . MSDs are shifted along the *y*-axis to enable better visualization, and *y*-axis scale is not the same in (a) and (b). $X_A = 0.1$, and variation of N_A is indicated in each figure.

of A beads is greater than that of B beads. It is therefore very likely that at even longer time scales MSDs of B beads would approach to those of A beads. However, for longer A chains ($N_{\rm A} = 20$ and 50), the slope of A beads' MSD is smaller than B beads' MSD at long time scales (see Figure 10b). Therefore,

when $N_{\rm A}$ > 20, A chains become fully effective obstacles for B chains across all time scales.

4.5.2. Effect of High- T_g Chain Concentration. Stiffening that is observed in mixed blend system could also be due to percolation of A chains. Therefore, the "burning method" was used to investigate if A chains percolate or not. It was found that percolation threshold $(N_{\rm p,A})$ in blends containing 5, 10, and 20% A chains were 20, 10, and 7, respectively. This is consistent with the fact that the percolation threshold for elongated objects is inversely proportional to the aspect ratio of the percolating objects, thus resulting in lower percolation thresholds for longer A chains.

To investigate whether the percolation of A chains is important to the stiffening mechanism, the storage moduli was calculated as a function of N_A for mixed blends at various volume fractions (X_A) (see Figure 11). For better visualization,

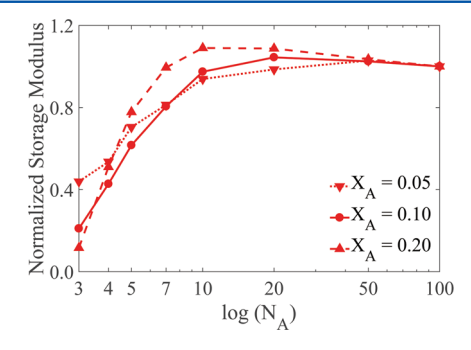


Figure 11. Normalized storage moduli of the mixed blends as a function of **A** chain length at $f = 0.001/\tau'$. Three curves represent various concentrations of **A** chains. All three curves were normalized with respect to their storage modulus at $N_{\rm A} = 100$.

each modulus value was normalized by the modulus of the N_A = 100 blend (at the same A chain concentration). It can be seen that at a constant A chain concentration increasing A chain length initially leads to increasing storage modulus. Just above the percolation threshold $(N_{\rm p,A})$, the storage modulus shows a maximum that is followed by a slight decrease. For blends containing 5, 10, and 20% A chains, the normalized storage modulus maximum was observed at N_A values of 50, 20, and 10, respectively. For reference, N_A values corresponding to the maximum storage modulus are named "critical chain length" and are labeled $N_{c,A}$. Interestingly, percolation threshold chain length $(N_{p,A})$ was found to be always smaller than the critical chain length $(N_{c,A})$. Therefore, it follows that (at a constant A chain concentration) increasing A chain length slightly above $N_{p,A}$ leads to the formation of a highly percolated and immobilized network. However, further increase in N_A , beyond the critical chain length, leads to decreasing normalized storage modulus because A chains themselves become softer (see Figure 2) with increasing N_A . In addition, as N_A is increased, the number of A-B contacts decreases (as discussed in section 4.5.1), which leads to further softening of the B chain matrix and to an overall decrease in the normalized storage modulus.

4.5.3. Effect of Chain Mobility. Viscoelastic properties of polymers depend on various factors. So far, our discussion included identifying the effect of static, dynamic, and viscoelastic properties. In order to investigate the role of A chain conformation separate from the interplay of chain dynamics, simulations were performed for the well-mixed, homogeneous blend system where the high- $T_{\rm g}$ A chains were not allowed to move ("frozen"). As such, in these simulations

frozen A chains act as static obstacles to the low- $T_{\rm g}$ B chains. It should be noted that A chains were frozen after full equilibration and production runs as explained previously.

The bead MSDs and non-Gaussianity parameters of low- $T_{\rm g}$ B chains are presented in Figure 12. Interestingly, the mobility of

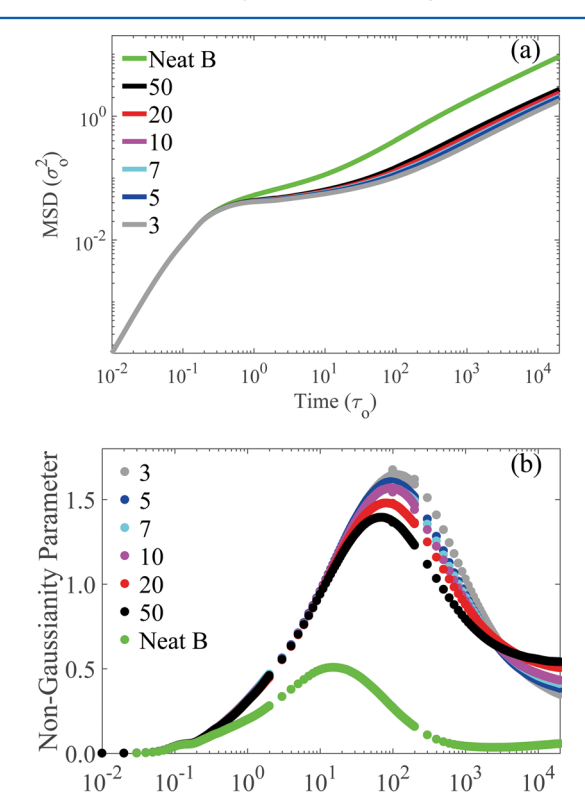


Figure 12. (a) MSD and (b) non-Gaussianity parameters of **B** beads in "frozen mixed" blends. Neat **B** melt result is also presented. $N_{\rm B}=50$ and $X_{\rm A}=0.1$ for blends.

the B beads is slowest in systems containing the shortest (frozen) A chains. This observation is opposite to that observed in the regular mixed systems (Figure 9a). The fact that shorter frozen A chains are more effective in immobilizing B chains than longer frozen A chains can be explained by statics alone—shorter A chains are stiffer (see Figure 2) and larger than their longer counterparts prior to being frozen, and therefore shorter chains have more number of A—B contacts.

Finally, Rouse mode relaxation power-law coefficient and relaxation time constants of B chains as a function of A chain length $(N_{\rm A})$ in regular mixed and frozen mixed blends are presented in Figure 13. The data show that the power-law coefficient and relaxation time constant of B chains in the frozen mixed systems approach values characterizing the regular mixed system in the limit of large $N_{\rm A}$. The dynamics of B chains in the frozen mixed and regular mixed blends become similar to increasing A chain length because as A chain length increases, frozen A chains become less effective obstacles to the dynamics of B chains as described in the previous paragraph.

5. SUMMARY AND CONCLUSIONS

Molecular dynamics simulations were performed on dynamically heterogeneous blend system consisting of soft (low- $T_{\rm g}$) and stiff (high- $T_{\rm g}$) polymer chains and having two distinct morphologies: homogeneous (well-dispersed, "mixed") and phase-separated ("unmixed"). The main finding of these

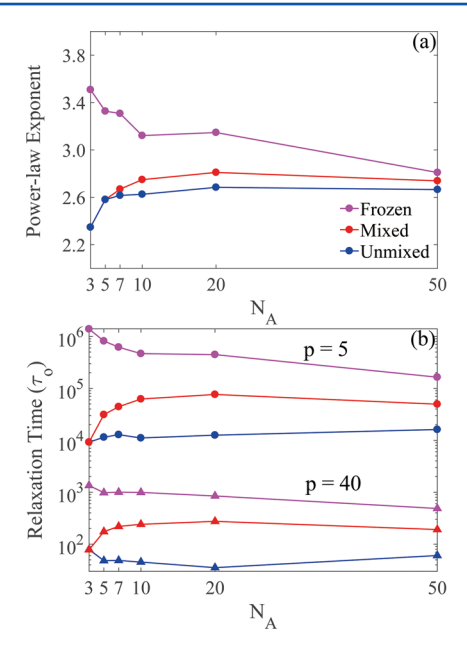


Figure 13. Dependence of (a) power-law exponent and (b) Rouse mode relaxation time constant as a function of **A** chain length in frozen mixed, regular mixed and unmixed blends. In (b) circles and triangles represent Rouse modes, p, of 5 and 40, respectively. $N_{\rm B} = 50$ and $X_{\rm A} = 0.1$ for blends.

simulations was obtained in oscillatory shear simulations performed at a temperature greater than the glass transition temperature $(T_{\rm g})$ of the matrix but lower than the $T_{\rm g}$ of the minor blend component. The storage modulus of the homogeneously mixed blends was greater than that of the phase-separated blends at all shear frequencies simulated. Analysis of various static and dynamics properties showed that the origin of this behavior was the ability of the high- $T_{\rm g}$ chains to slow down the dynamics of the low- $T_{\rm g}$ matrix chains due to greater number of interactions between the two chain types in the mixed state.

By investigating the role of the high- $T_{\rm g}$ chain length and the associated dynamics, it was determined that decreasing mobility of the high- $T_{\rm g}$ chains was the major factor determining the degree of stiffening. With increasing high- $T_{\rm g}$ chain length, a percolated high- $T_{\rm g}$ chain network was formed in the homogeneously mixed blend, whereas percolation was never observed in the phase-separated blend. The highly connected percolated network of high- $T_{\rm g}$ chains led to a complete immobilization of the high- $T_{\rm g}$ polymer network, and no further stiffening was observed with increasing high- $T_{\rm g}$ chain length.

Interestingly, it was observed that even relatively short high- $T_{\rm g}$ chains $(N_{\rm A} \sim 5{-}10)$ were capable of significantly immobilizing low- $T_{\rm g}$ matrix chains. This finding indicates that one can stiffen polymer melts with relatively small, but rigid macromolecules.

AUTHOR INFORMATION

Corresponding Author

*E-mail ozisik@rpi.edu (R.O.).

ORCID ®

Wei Peng: 0000-0002-4232-501X

Notes

The authors declare no competing financial interest.

ACKNOWLEDGMENTS

This material is partially based upon work supported by the National Science Foundation under Grant CMMI-1538730.

REFERENCES

- (1) Vlassopoulos, D.; Koumoutsakos, A.; Anastasiadis, S. H. Rheology and Phase Separation in a Model Upper Critical Solution Temperature Polymer Blend. *J. Rheol.* **1997**, *41*, 739–755.
- (2) Kapnistos, M.; Hinrichs, A.; Vlassopoulos, D.; Anastasiadis, S. H.; Stammer, A.; Wolf, B. A. Rheology of a Lower Critical Solution Temperature Binary Polymer Blend in the Homogeneous, Phase-Separated, and Transitional Regimes. *Macromolecules* **1996**, *29*, 7155–7163.
- (3) Khademzadeh Yeganeh, J.; Goharpey, F.; Foudazi, R. Rheology and Morphology of Dynamically Asymmetric LCST Blends: Polystyrene/poly(vinyl Methyl Ether). *Macromolecules* **2010**, *43*, 8670–8685.
- (4) Pathak, J. A.; Colby, R. H.; Kamath, S. Y.; Kumar, S. K.; Stadler, R. Rheology of Miscible Blends: SAN and PMMA. *Macromolecules* **1998**, *31*, 8988–8997.
- (5) Ajji, A.; Choplin, L. Rheology and Dynamics near Phase Separation in a Polymer Blend: Model and Scaling Analysis. *Macromolecules* **1991**, *24*, 5221–5223.
- (6) Kioupis, L. I.; Maginn, E. J. Rheology, Dynamics, and Structure of Hydrocarbon Blends: A Molecular Dynamics Study of N-Hexane/n-Hexadecane Mixtures. *Chem. Eng. J.* 1999, 74, 129–146.
- (7) Fredrickson, G. H.; Larson, R. G. Viscoelasticity of Homogeneous Polymer Melts near a Critical Point. *J. Chem. Phys.* **1987**, *86*, 1553–1560.
- (8) Ngai, K. L.; Capaccioli, S. Unified Explanation of the Anomalous Dynamic Properties of Highly Asymmetric Polymer Blends. *J. Chem. Phys.* **2013**, *138*, 054903.
- (9) Colmenero, J. A Generalized Rouse Incoherent Scattering Function for Chain Dynamics of Unentangled Polymers in Dynamically Asymmetric Blends. *Macromolecules* **2013**, *46*, 5363–5370.
- (10) Slimani, M. Z.; Moreno, A. J.; Rossi, G.; Colmenero, J. Dynamic Heterogeneity in Random and Gradient Copolymers: A Computational Investigation. *Macromolecules* **2013**, *46*, 5066–5079.
- (11) Brodeck, M.; Alvarez, F.; Colmenero, J.; Richter, D. Single Chain Dynamic Structure Factor of Poly(ethylene Oxide) in Dynamically Asymmetric Blends with Poly(methyl Methacrylate). Neutron Scattering and Molecular Dynamics Simulations. *Macromolecules* **2012**, *45*, 536–542.
- (12) Bernabei, M.; Moreno, A. J.; Colmenero, J. Static and Dynamic Contributions to Anomalous Chain Dynamics in Polymer Blends. *J. Phys.: Condens. Matter* **2011**, 23, 234119.
- (13) Diddens, D.; Brodeck, M.; Heuer, A. Microscopic Understanding of the Complex Polymer Dynamics in a Blend —A Molecular-Dynamics Simulation Study. *EPL (Europhysics Lett)*. **2011**, 95, 56003.
- (14) Ngai, K. L.; Wang, L. M. Interchain Coupled Chain Dynamics of Poly(ethylene Oxide) in Blends with Poly(methyl Methacrylate): Coupling Model Analysis. *J. Chem. Phys.* **2011**, *135*, 194902.
- (15) Brodeck, M.; Alvarez, F.; Moreno, A. J.; Colmenero, J.; Richter, D. Chain Motion in Nonentangled Dynamically Asymmetric Polymer Blends: Comparison between Atomistic Simulations of PEO/PMMA and a Generic Bead-Spring Model. *Macromolecules* **2010**, *43*, 3036–3051.
- (16) Moreno, A. J.; Colmenero, J. Entangledlike Chain Dynamics in Nonentangled Polymer Blends with Large Dynamic Asymmetry. *Phys. Rev. Lett.* **2008**, *100*, 1–4.
- (17) Moreno, A. J.; Colmenero, J. Tests of Mode Coupling Theory in a Simple Model for Two-Component Miscible Polymer Blends. *J. Phys.: Condens. Matter* **2007**, *19*, 466112.
- (18) Niedzwiedz, K.; Wischnewski, A.; Monkenbusch, M.; Richter, D.; Genix, A. C.; Arbe, A.; Colmenero, J.; Strauch, M.; Straube, E.

Polymer Chain Dynamics in a Random Environment: Heterogeneous Mobilities. *Phys. Rev. Lett.* **2007**, *98*, 1–4.

- (19) Moreno, A. J.; Colmenero, J. Is There a Higher-Order Mode Coupling Transition in Polymer Blends? *J. Chem. Phys.* **2006**, *124*, 184906.
- (20) Bedrov, D.; Smith, G. D. Macromolecules 2006, 39, 8526-8535.
- (21) Bedrov, D.; Smith, G. D. A Molecular Dynamics Simulation Study of Relaxation Processes in the Dynamical Fast Component of Miscible Polymer Blends. *Macromolecules* **2005**, *38*, 10314–10319.
- (22) Genix, A.-C.; Arbe, A.; Alvarez, F.; Colmenero, J.; Willner, L.; Richter, D. Dynamics of Poly(ethylene Oxide) in a Blend with Poly(methyl Methacrylate): A Quasielastic Neutron Scattering and Molecular Dynamics Simulations Study. *Phys. Rev. E* **2005**, *72*, 31808.
- (23) Leroy, E.; Alegría, A.; Colmenero, J. Segmental Dynamics in Miscible Polymer Blends: Modeling the Combined Effects of Chain Connectivity and Concentration Fluctuations. *Macromolecules* **2003**, 36, 7280–7288.
- (24) Salaniwal, S.; Kant, R.; Colby, R. H.; Kumar, S. K. Computer Simulations of Local Concentration Variations in Miscible Polymer Blends. *Macromolecules* **2002**, *35*, 9211–9218.
- (25) Kamath, S.; Colby, R. H.; Kumar, S. K.; Karatasos, K.; Floudas, G.; Fytas, G.; Roovers, J. E. L. Segmental Dynamics of Miscible Polymer Blends: Comparison of the Predictions of a Concentration Fluctuation Model to Experiment. *J. Chem. Phys.* **1999**, *111*, 6121.
- (26) Kanaya, T.; Tsukushi, I.; Kaji, K. Non-Gaussian Parameter and Heterogeneity of Amorphous Polymers. *Prog. Theor. Phys. Suppl.* **1997**, 126, 133–140.
- (27) Kremer, K.; Grest, G. S. Dynamics of Entangled Linear Polymer Melts: A Molecular-Dynamics Simulation. *J. Chem. Phys.* **1990**, *92*, 5057–5086.
- (28) Schweizer, K. S. Microscopic Theory of the Dynamics of Polymeric Liquids: General Formulation of a Mode Mode-Coupling Approach. *J. Chem. Phys.* **1989**, *91*, 5802–5821.
- (29) Senses, E.; Isherwood, A.; Akcora, P. Reversible Thermal Stiffening in Polymer Nanocomposites. *ACS Appl. Mater. Interfaces* **2015**, *7*, 14682–14689.
- (30) Doi, M.; Edwards, S. F. The Theory of Polymer Dynamics; Oxford Science Publications: 1986.
- (31) Kalathi, J. T.; Kumar, S. K.; Rubinstein, M.; Grest, G. S. Rouse Mode Analysis of Chain Relaxation in Homopolymer Melts. *Macromolecules* **2014**, *47*, 6925–6931.
- (32) Kremer, K.; Grest, G. S.; Carmesin, I. Crossover from Rouse to Reptation Dynamics: A Molecular-Dynamics Simulation. *Phys. Rev. Lett.* **1988**, *61*, 566–569.
- (33) Everaers, R.; Sukumaran, S. K.; Grest, G. S.; Svaneborg, C.; Sivasubramanian, A.; Kremer, K. Rheology and Microscopic Topology of Entangled Polymeric Liquids. *Science (Washington, DC, U. S.)* **2004**, 303, 823–826.
- (34) Sukumaran, S. K.; Grest, G. S.; Kremer, K.; Everaers, R. Identifying the Primitive Path Mesh in Entangled Polymer Liquids. *J. Polym. Sci., Part B: Polym. Phys.* **2005**, 43, 917–933.
- (35) Kalathi, J. T.; Grest, G. S.; Kumar, S. K. Universal Viscosity Behavior of Polymer Nanocomposites. *Phys. Rev. Lett.* **2012**, *109*, 1–5.
- (36) Plimpton, S. Fast Parallel Algorithms for Short-Range Molecular Dynamics. *J. Comput. Phys.* **1995**, *117*, 1–19.
- (37) Stukowski, A. Visualization and Analysis of Atomistic Simulation Data with OVITO—the Open Visualization Tool. *Modell. Simul. Mater. Sci. Eng.* **2010**, *18*, 015012.
- (38) Sen, S.; Kumar, S.; Keblinski, P. Viscoelastic Properties of Polymer Melts from Equilibrium Molecular Dynamics Simulations. *Macromolecules* **2005**, *38*, 650–653.
- (39) Evans, D. J.; Morriss, G. P. Nonlinear-Response Theory for Steady Planar Couette Flow. *Phys. Rev. A: At., Mol., Opt. Phys.* **1984**, 30, 1528–1530.
- (40) Lees, A. W.; Edwards, S. F. The Computer Study of Transport Processes under Extreme Conditions. *J. Phys. C: Solid State Phys.* **1972**, 5, 1921–1929.
- (41) Arrese-Igor, S.; Alegría, A.; Moreno, A. J.; Colmenero, J. Effect of Blending on the Chain Dynamics of The "low-Tg" component in

Nonentangled and Dynamically Asymmetric Polymer Blends. *Macromolecules* **2011**, *44*, 3611–3621.

- (42) Sakai, V. G.; Maranas, J. K.; Peral, I.; Copley, J. R. D. Dynamics of PEO in Blends with PMMA: Study of the Effects of Blend Composition via Quasi-Elastic Neutron Scattering. *Macromolecules* **2008**, *41*, 3701–3710.
- (43) Urakawa, O.; Ujii, T.; Adachi, K. Dynamic Heterogeneity in a Miscible Poly(vinyl Acetate)/poly(ethylene Oxide) Blend. *J. Non-Cryst. Solids* **2006**, 352, 5042–5049.
- (44) El Mabrouk, K.; Bousmina, M. Effect of Hydrodynamics on Dynamics of Phase Separation in Polystyrene/poly(vinyl Methyl Ether) Blend. *Polymer* **2005**, *46*, 9005–9014.
- (45) Sakai, V. G.; Maranas, J. K.; Chowdhuri, Z.; Peral, I.; Copley, J. R. D. Miscible Blend Dynamics and the Length Scale of Local Compositions. *J. Polym. Sci., Part B: Polym. Phys.* **2005**, 43, 2914–2923.
- (46) Kumar, S. K.; Colby, R. H.; Anastasiadis, S. H.; Fytas, G. Introduction, I. Concentration Fluctuation Induced Dynamic Heterogeneities in Polymer Blends. *J. Chem. Phys.* **1996**, *105*, 3777–3788.
- (47) Katana, G.; Fischer, E. W.; Hack, T.; Abetz, V.; Kremer, F. Influence of Concentration Fluctuations on the Dielectric α-Relaxation in Homogeneous Polymer Mixtures. *Macromolecules* **1995**, 28, 2714–2722.
- (48) Herrmann, H.; Hong, D.; Stanley, H. Backbone and Elastic Backbone of Percolation Clusters Obtained by the New Method Ofburning'. J. Phys. A: Math. Gen. 1984, 17, L261.
- (49) Sahimi, M. Application of Percolation Theory; Taylor & Francis Ltd.: 1994.